JTE HCM-UTE
ISSN: 2615-9740

JOURNAL OF TECHNICAL EDUCATION SCIENCE
Ho Chi Minh City University of Technology and Engineering
Website: https://jte.edu.vn
Email: jte@hcmute.edu.vn

Modeling Carbon-Nanotube-Based Nano-Electro-Mechanical Systems for Application in Mass Detection Sensors

Dai D. Mai[1*], Tuan D. Vu[2], Si T. Do[3]
[1]*Ho Chi Minh City University of Technology and Engineering, Vietnam*
[2]*Vietnam-Korea Binh Duong College, Vietnam*
[3]*FPT Polytechnic, FPT University, Vietnam*

[*]Corresponding author. *Email: daimd@hcmute.edu.vn*

ARTICLE INFO

Received: 12/04/2026
Revised: 24/04/2026
Accepted: 13/05/2026
Online First: 29/05/2026
Published:

KEYWORDS

Nano-electro-mechanical systems;
Coupled field finite element method;
Electrostatic tuning;
Carbon-nanotube resonator;
Pull in instability.

ABSTRACT

Carbon nanotube-based nano-electro-mechanical systems (NEMS) have emerged as highly promising platforms for ultrasensitive mass detection and nanoscale signal processing. This paper presents a comprehensive investigation of the resonance behavior, tunability, and instability thresholds of such devices under electrostatic actuation and mass loading. A coupled electro-mechanical finite-element model is developed, wherein the nanotube is represented by shell elements, electrostatic actuation is modeled via reduced-order transducer elements, and adsorbed particles are introduced through lumped mass elements. The proposed model is rigorously validated against beam-theory results and published molecular-dynamics data, yielding mean errors of 1.02%–2.39%. Parametric studies demonstrate strong voltage tuning; for a baseline device, the fundamental frequency rises significantly from 549.28 MHz (0 V) to 2108.1 MHz (60 V). Furthermore, the analysis reveals a geometry-dependent pull-in limit and confirms that mass adsorption causes a commensurate reduction in resonant frequency. Geometrically nonlinear analysis also predicts a higher instability threshold compared to linear models. Ultimately, these findings validate a compact and effective design framework for optimizing CNT geometry and bias conditions in tunable NEMS mass sensors.

Doi: https://doi.org/10.54644/jte.2026.2294

1. Introduction

Nanomechanical resonators are established transducers for biological and chemical detection because adsorption-induced resonance changes can encode added mass, interaction kinetics, proteolysis, and surface-stress effects. Eom et al. synthesized the governing nanomechanics [1], while subsequent studies demonstrated direct tracking of biomolecular binding kinetics [2], in-situ peptide proteolysis [3], and surface-stress-driven dynamic responses [4].

Within this field, carbon-nanotube (CNT) resonators remain especially attractive because their exceptionally low inertial mass and high stiffness can generate pronounced frequency shifts under minute perturbations. Prior CNT studies clarified the roles of finite kinematics and charge concentration in electrostatically actuated nanotube NEMS [5], analyzed the resonant response to DNA binding [6], and developed continuum-based mass-sensing models for multi-walled CNT (MWCNT) resonators [7]. The present work extends this last line by adopting the single-equivalent-shell (SES) continuum approximation, in which the multi-walled stack is represented as a single shell whose dynamic response is dominated by synchronous in-phase vibration of all walls under the inter-wall van-der-Waals coupling [8], [9]. This approximation is well established for the fundamental flexural-mode regime of MWCNT resonators (MHz–GHz), where out-of-phase modes lie at THz frequencies and are not excited [8], [10], [11]; it captures the design-relevant dynamics with a small fraction of the computational cost of an explicit multi-shell formulation. The present work extends this last line, specifically, the single-equivalent-shell continuum framework, into a fully coupled electro-mechanical setting in ANSYS.

Recent work has further consolidated the field along two complementary directions. On the experimental side, ultra-low-mass CNT resonators have demonstrated single-molecule and even sub-proton mass resolution under cryogenic operation [12]–[14], and room-temperature CNT mass sensors continue to push the trade-off between quality factor, bandwidth, and detectable mass [15]. On the modelling side, four main routes are now used to describe CNT vibration: classical Euler-Bernoulli or Timoshenko beam theory, continuum shell theory in either the single-equivalent-shell or multi-shell formulations [7], [8]–[11], nonlocal-elasticity and modified-couple-stress formulations that introduce an internal length scale [16]. The present coupled-field continuum-shell framework is positioned within this landscape as a design-oriented compromise that retains the fidelity of the shell formulation while keeping the computational cost compatible with parametric design sweeps, and it is implemented within a single ANSYS workflow [15].

Building on the elements above, the present study develops a unified coupled-field finite-element framework for MWCNT-based NEMS resonators using continuum shell elements (within the single-equivalent-shell approximation) for the nanotube, reduced-order transducer elements for electrostatic actuation, and lumped masses for adsorbates. The contributions of this work are threefold: (i) a unified ANSYS workflow that combines shell mechanics, reduced-order electrostatic actuation, and adsorbate mass loading for MWCNT-NEMS; (ii) a joint analysis of higher-mode voltage tuning together with pull-in stability; and (iii) a quantitative linear vs. geometrically nonlinear comparison that yields a practical bias-selection margin for sensor design [17], [18].

2. Modeling mass detection sensors based on NEMS

This section defines the computational model used in the study. The formulation couples the structural representation of the CNT, electrostatic actuation, adsorbed-mass loading, and finite-element implementation used to obtain the resonance and pull-in results.

2.1. Modeling carbon-nanotube-based NEMS

Several approaches have been proposed to describe CNT mechanics, and they can be grouped into three main categories: atomistic modeling, molecular structural mechanics, and continuum elastic modeling.

Atomistic modeling provides the most detailed description of CNT behavior because it resolves the mechanical response directly at the atomic scale. However, it also presents several practical limitations:

- It becomes computationally impractical for long CNTs because the number of atoms increases very rapidly;
- The computational cost is therefore extremely high and often exceeds the capability of standard computing systems;
- The formulation also requires treatment of advanced physical effects, including electromechanical and quantum-scale phenomena.

Molecular structural mechanics (MSM) reduces this complexity by replacing C-C atomic bonds with equivalent mechanical elements. This approach extends the accessible CNT length range while retaining the discrete character of the structure, although the resulting models can still be computationally demanding.

Continuum elastic models, widely used in engineering applications, treat CNTs as equivalent beams or shells. Although atomistic detail is no longer resolved explicitly, this approach offers a practical balance between physical fidelity and computational efficiency for design-oriented simulations. Based on this tradeoff, the present work adopts a continuum shell-based FEM strategy; the scale dependence of alternative CNT modeling approaches is summarized in Figure 1.

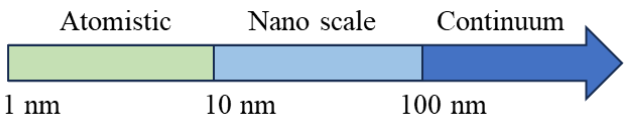

Figure 1. *Modeling methods used for CNTs at different scales.*

2.2. Modeling electro-mechanical interaction

The equation of motion for forced vibrations of the MWCNT couples elastic, electrostatic, and van-der-Waals (vdW) contributions. Following the continuum-shell formulation in [5], [7], the governing equation:

$$EI\frac{d^4w(x,t)}{dx^4}-\frac{EA}{2L}\int_0^L\left(\frac{dw(x,t)}{dx}\right)^2dx\frac{d^2w(x,t)}{dx^2}+\rho(x,t)dx\frac{d^2w(x,t)}{dt^2}=q_{elec}+q_{vdW} \quad (1)$$

When the MWCNT electrode gap exceeds about 10 nm, the vdW pressure between the tube and the electrode scales as $\sim 1/D^4$ and falls below 1% of the electrostatic pressure for the bias range considered here, consistent with the estimate in [5]; therefore the q_{vdW} term in Eq. (1) is neglected, and the equation simplifies to:

$$EI\frac{d^4w}{dx^4}-\frac{EA}{2L}\int_0^L\left(\frac{dw}{dx}\right)^2dx\frac{d^2w}{dx^2}+\rho(x,t)dx\frac{d^2w(x,t)}{dt^2}=q_{elec} \quad (2)$$

The distributed electrostatic force per unit length, q_{elec}, follows the parallel-cylinder/plane formulation [5], [17]:

$$q_{elec}=\frac{1}{2}V^2\frac{dC}{dr}=\frac{\pi\varepsilon_oV^2}{\sqrt{r(r+2R_{ext})}arccosh^2\left(1+\frac{r}{R_{ext}}\right)} \quad (3)$$

where r = D − w(x,t) is the instantaneous MWCNT–electrode distance. The distributed mass density is

$$\rho(x,t)=\rho_{CNT}A+\Delta m(x).H(t-t_0) \quad (4)$$

where $\Delta m(x)$ denotes the mass of adsorbed particles, t_0 is the time at which particle adsorption takes place, and $H(t)$ is the Heaviside function indicating the moment of particle attachment.

Substituting the relevant variables and simplifying, the governing equation becomes:

$$EI\frac{d^4w}{dx^4}-\frac{EA}{2L}\int_0^L\left(\frac{dw}{dx}\right)^2dx\frac{d^2w}{dx^2}+\rho(x,t)dx\frac{d^2w(x,t)}{dt^2}=\frac{\pi\varepsilon_oV^2}{\sqrt{\big(D-w(x,t)\big)(D-w(x,t)+2R_{ext})}arccosh^2\left(1+\frac{D-w(x,t)}{R_{ext}}\right)} \quad (5)$$

When both a DC voltage and an AC voltage are applied simultaneously to the electrode, the resulting electrostatic excitation consists of a steady component and a time-varying (harmonic) component. The total applied voltage is expressed as:

$$V=V_{DC}+V_{AC}\,sin(\omega t) \quad (6)$$

From the Eq. (3) and (4) the electrostatic force becomes:

$$\begin{aligned}q_{elec}=\frac{1}{2}V^2\frac{dC}{dr}&=\frac{\pi\varepsilon_o(V_{DC}^2+2V_{DC}V_{AC}\,sin\,(\omega t)\;+V_{AC}^2\,sin\,(\omega t)^2\,)}{\sqrt{\big(D-w(x,t)\big)(D-w(x,t)+2R_{ext})}arccosh^2\left(1+\frac{D-w(x,t)}{R_{ext}}\right)}\\&=\frac{\pi\varepsilon_o\left(V_{DC}^2+\frac{1}{2}V_{AC}^2+2V_{DC}V_{AC}\,sin\,(\omega t)\;-\frac{1}{2}V_{AC}^2\,sin\,(2\omega t)^2\,\right)}{\sqrt{\big(D-w(x,t)\big)(D-w(x,t)+2R_{ext})}arccosh^2\left(1+\frac{D-w(x,t)}{R_{ext}}\right)}\end{aligned} \quad (7)$$

Since the magnitude of the AC voltage is typically much smaller than that of the DC voltage, higher-order harmonic terms can be neglected. Thus, the simplified electrostatic force expression is:

$$q_{elec} = \frac{\pi\varepsilon_o\left(V_{DC}^2 + \frac{1}{2}V_{AC}^2 + 2V_{DC}V_{AC}\,sin\,(\omega t)\right)}{\sqrt{(D - w(x,t))(D - w(x,t) + 2R_{ext})}\,arccosh^2\left(1 + \frac{D - w(x,t)}{R_{ext}}\right)} \tag{8}$$

Finally, substituting Eq. (8) into Eq. (5) yields the governing equation of motion for the NEMS system under electrostatic excitation:

$$EI\frac{d^4w}{dx^4} - \frac{EA}{2L}\int_0^L \left(\frac{dw}{dx}\right)^2 dx\frac{d^2w}{dx^2} + \rho(x,t)dx\frac{d^2w(x,t)}{dt^2}$$
$$= \frac{\pi\varepsilon_o\left(V_{DC}^2 + \frac{1}{2}V_{AC}^2 + 2V_{DC}V_{AC}\,sin\,(\omega t)\right)}{\sqrt{(D - w(x,t))(D - w(x,t) + 2R_{ext})}\,arccosh^2\left(1 + \frac{D - w(x,t)}{R_{ext}}\right)} \tag{9}$$

When the excitation frequency approaches the natural frequency of the CNT structure, resonance may occur, leading to a significant increase in amplitude. This phenomenon is critical in mass sensing applications, where frequency shifts due to mass adsorption are used to infer the presence and quantity of target particles.

2.3. Finite Element Modeling of NEMS-Based Mass Detection Sensors in ANSYS

The MWCNT-NEMS mass sensor is modelled in ANSYS (Figure 2) as a doubly-clamped MWCNT of length L, outer radius R, and equivalent wall thickness t, with an adsorbate at axial position X_m. The MWCNT mechanics is discretised with SHELL181, a four-node shell element capturing both bending and membrane responses [15]. Electro-mechanical coupling is represented by TRANS126 reduced-order transducer elements [15], and the adsorbed particle is introduced through a MASS21 lumped mass placed at the adsorption site. This combination allows the dynamic effect of local mass loading on the natural frequency to be evaluated directly within a single coupled-field workflow.

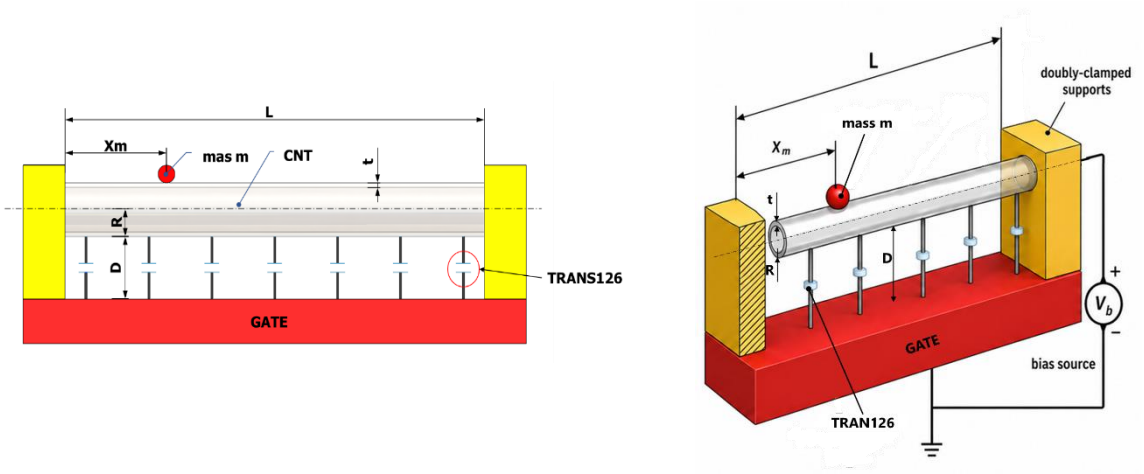

(a) Cross-sectional schematic (b) 3D isometric view

Figure 2. *Finite-element model of the MWCNT-NEMS mass-detection sensor.*

Implementation-wise, the TRANS126 elements are connected between an electrode-side fixed node and pilot nodes constrained to follow the radial displacement of the bottom-surface MWCNT shell nodes; the MASS21 element is attached at the corresponding shell node at the adsorption site by sharing the node ID.

The continuum-shell parameter set follows the single-equivalent-shell (SES) convention, which has been validated for the fundamental flexural modes of MWCNTs [7], [14]–[17]. The model incorporates a representative wall thickness alongside standard graphene-sheet material constants, $E = 1.0\,\text{TPa}, \nu = 0.16$, and $\rho = 2300\,\text{kg/m}^3$. Within the SES framework, these parameters were calibrated against the continuum mass-sensing data published by Choi et al. for MWCNT resonators of

similar geometry [7]. As detailed in Section 1, the van der Waals (vdW)-locked synchronous-vibration mechanism ensures that this single-shell continuum representation accurately captures the dynamic response of the multi-walled stack at the fundamental flexural frequencies of interest.

The next section first validates the model and then examines how the resonant response varies with MWCNT length, adsorbed mass magnitude, adsorption position, applied bias, and pull-in stability.

3. Results and Discussion

3.1. Model Validation

The proposed coupled-field shell FEM was validated by comparing its natural frequencies with Euler-Bernoulli beam theory and with independent published CNT/MWCNT benchmark data [7], [8]. Instead of plotting the absolute frequencies, the comparison is reported in terms of the relative frequency deviation,

$$\Delta f_n = 100\left(f_{n,FEM} - f_{n,EB}\right)/f_{n,EB} \tag{10}$$

where $f_{n,EB}$ is the Euler-Bernoulli prediction for the same mode. This representation makes the validation more stringent because it directly exposes the departure of the shell-FEM solution from the beam-theory limit.

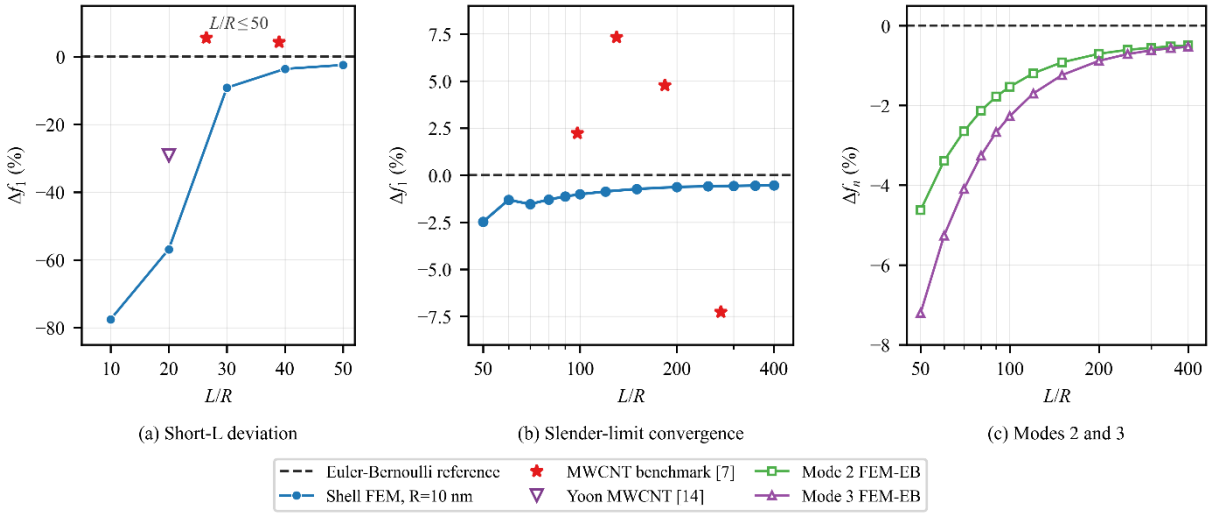

Figure 3. *Validation of the proposed shell FEM against Euler–Bernoulli beam theory and published CNT/MWCNT benchmark data [7], [8].*

Figure 3 separates the validation into three regimes. In the short-length regime, Figure 3(a), additional MAPDL shell-FEM calculations were performed for the same $R = 10$ nm nanotube geometry at $L/R = 10, 20, 30, 40,$ and 50. The mode-1 deviation is no longer close to zero; it changes from -77.52% at $L/R = 10$ to -2.47% at $L/R = 50$. This visible divergence directly addresses the reviewer's concern that a validation plot showing coincident FEM and beam-theory mode-1 curves is not meaningful. The overlaid CNT/MWCNT benchmark markers from the literature [7], [8] are not treated as point-by-point same-geometry error data, but they provide an independent reference showing that appreciable departures from the Euler-Bernoulli limit are expected in low-slenderness CNT/MWCNT resonators.

For the long-tube MWCNT sweep with $R = 10$ nm, $t = 0.34$ nm, and $L = 500 - 4000$ nm, Figure 3(b) shows the expected convergence toward Euler-Bernoulli behavior as L/R increases. The signed mode-1 deviation varies from -2.47% at $L/R = 50$ to -0.54% at the largest slenderness ratio, with a mean absolute deviation of 1.02%. Thus, the near-coincidence between FEM and Euler-Bernoulli theory in the slender limit is used only as an implementation consistency check, while the substantive validation is provided by the short-L divergence in Figure 3(a) together with the independent literature benchmarks [7], [8].

Figure 3(c) gives an additional check for Mode 2 and 3 over the same long-tube sweep. The deviations are larger for higher modes, ranging from -4.63% to -0.49% for mode 2 and from -7.21% to -0.53% for mode 3. This trend is physically reasonable because higher modes are more sensitive to finite wall thickness, shell bending, rotary inertia, and shear-deformation effects that are not represented in the Euler-Bernoulli approximation. Overall, the validation demonstrates both the correct convergence of the proposed shell-FEM model to beam theory in the slender-beam limit and its non-trivial departure from beam theory in the short-tube regime.

3.2. Harmonic response of NEMS

For the baseline harmonic analysis, the device parameters are $L = 1000$ nm, $H = 100$ nm, and $R = 10$ nm. The corresponding frequency-response curves under different bias conditions are shown in Figure 4.

The frequency shift is defined as $\Delta\omega = \omega_n - \omega_0$, where ω_n is the resonant frequency under applied voltage and ω_0 is the zero-bias reference value. For the two representative biased cases, the shifts are $\Delta\omega_1 = 45.65$ MHz and $\Delta\omega_2 = 204.52$ MHz, respectively. These results show that increasing the electrode voltage raises both the vibration amplitude and the resonant frequency of the device.

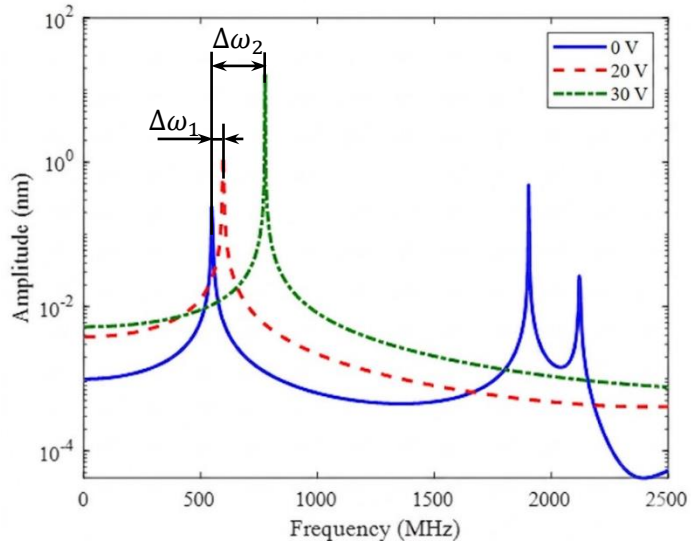

Figure 4. *Frequency harmonic response in NEMS under the effect of voltage.*

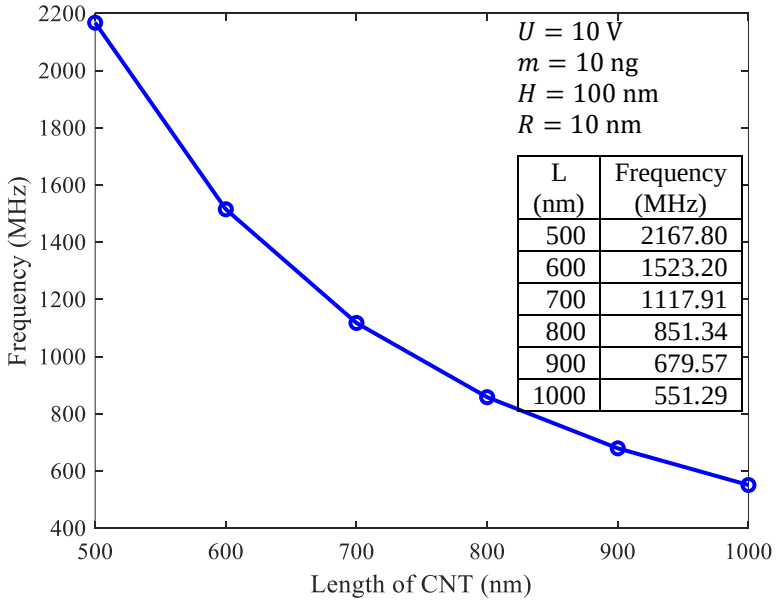

Figure 5*. Evolution of vibration frequency depends on the length of the CNT.*

3.3. Relationship Between Resonant Frequency and CNT Length

MWCNT length is a key design variable for the proposed sensor. In this analysis, L varies from 500 nm to 1000 nm, while $D = 100$ nm, $R = 10$ nm, $V_{DC} = 10$ V, $V_{AC} = 0$, and the adsorbed mass $m = 10$ ng is fixed at the mid-span ($X_m = L/2$).

As shown in Figure 5, increasing the MWCNT length lowers the resonant frequency from approximately 2167.80 MHz at $L = 500$ nm to 551.29 MHz at $L = 1000$ nm. Shorter MWCNTs therefore provide higher operating frequencies and stronger sensitivity to added mass, which explains the continued interest in miniaturised CNT resonators [12]–[15]. It should be noted that, at very small length scales, nonlocal-elasticity and modified-couple-stress effects can become non-negligible [16]; the present continuum-shell results remain consistent with the regime where local-elasticity assumptions are widely accepted, and a full nonlocal/couple-stress comparison is identified as an additional direction for future work.

3.4. Relationship between Resonant Frequency and Adsorbed Mass

To evaluate mass loading, $L = 1000$ nm, $H = 100$ nm, $R = 10$ nm are fixed. The adsorbed mass is placed at the midpoint $L/2$. The frequency shift is defined as $\Delta\omega = \Delta\omega_m - \Delta\omega_0$, where ω_m is the resonant frequency after mass adsorption, and ω_0 is the baseline frequency without mass.

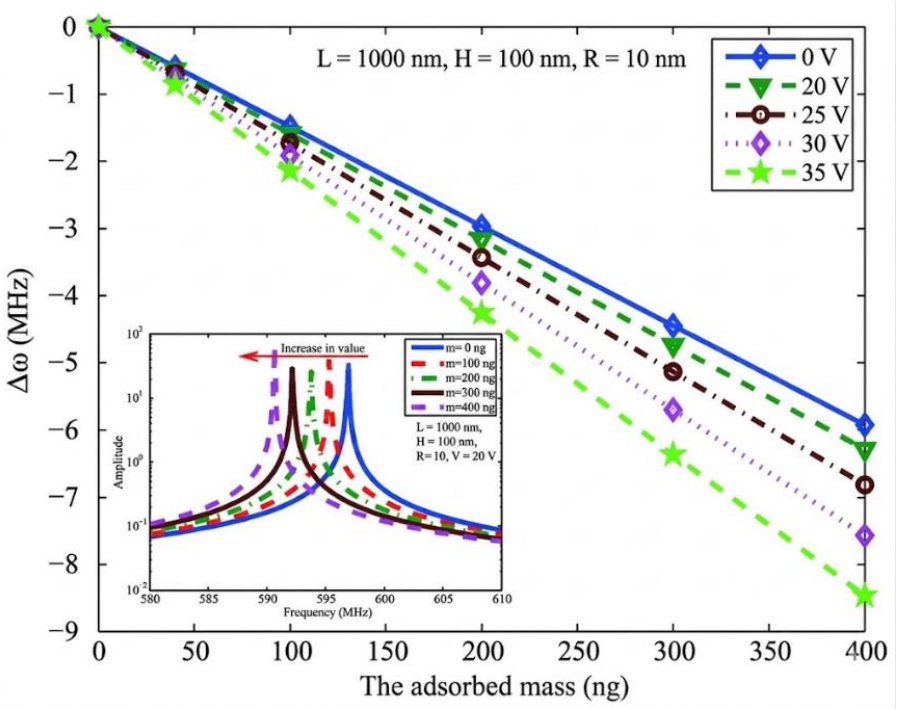

Figure 6. *The frequency shift follows adsorbed mass in CNT at different voltages.*

Figure 6 shows that the resonant frequency decreases monotonically as the adsorbed mass increases, confirming the high mass sensitivity of the CNT resonator. The magnitude of the shift also increases with applied voltage, indicating that electrostatic bias can improve signal resolution. This trend is consistent with earlier nanomechanical biosensing studies that monitored biomolecular interactions and proteolytic reactions through adsorption-induced frequency changes [2], [3].

3.5. Effect of Adsorbed Mass Position on Resonance Frequency

The adsorption position is another important parameter in sensor performance. Figure 7 plots the frequency shift $\Delta\omega_x = \omega_x - \omega_0$ as the adsorbed mass moves along the CNT from 0 to 1000 nm.

The largest frequency shift occurs when the adsorbed mass is near the CNT midpoint, whereas masses near the clamped ends produce much smaller shifts. This position dependence should be taken into account when interpreting sensor output and selecting adsorption locations.

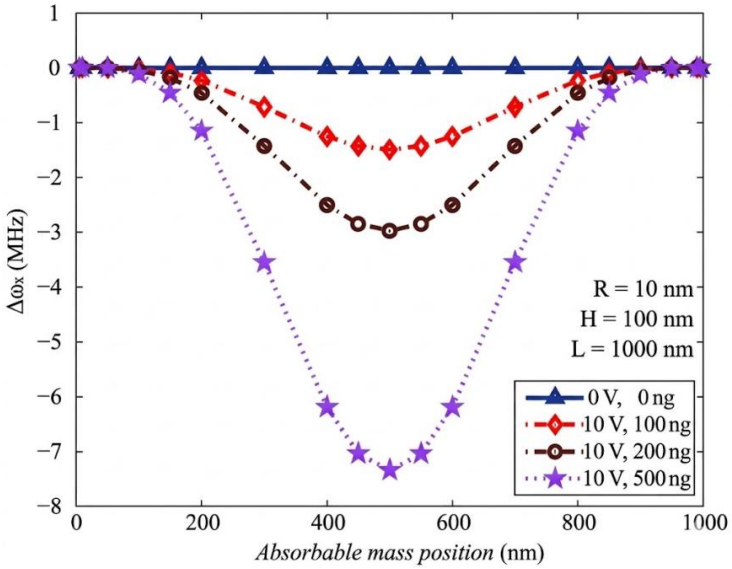

Figure 7. *Resonance frequency shift as a function of adsorbed-mass position.*

3.6. Electrostatic Tuning of Higher Modes

Figure 8 shows that the same FEM model also predicts strong DC-bias tuning of the first three modes. For the baseline device, the first mode rises from 549.28 MHz at 0 V to 2108.1 MHz at 60 V, while the second and third modes increase from 1505.0 MHz to 4981.5 MHz and from 2927.7 MHz to 8138.5 MHz, respectively (Figure 8). This trend is consistent with electrostatic stiffening mechanisms in CNT-NEMS [5].

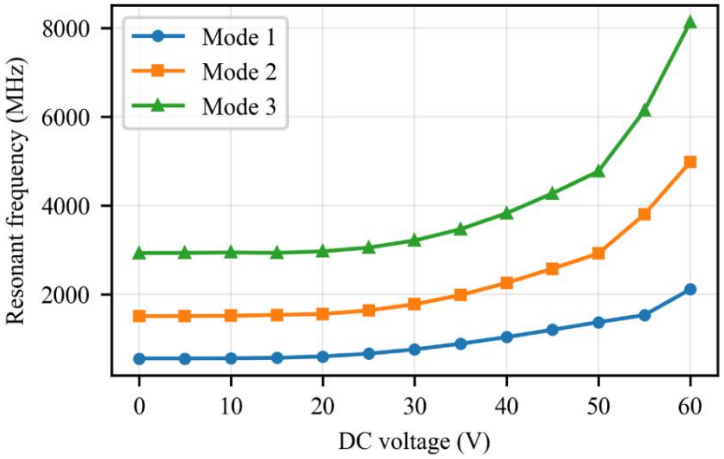

Figure 8. *Voltage-dependent tuning of the first three resonant modes for the baseline CNT-NEMS device.*

3.7. Static Stability and Pull-in Voltage

The steady state coupled field simulations show that the pull in voltage decreases from about 72 V at $L = 1000$ nm to 9 V at $L = 4000$ nm, but increases with both the initial gap and the tube radius, consistent with prior CNT-NEMS pull-in studies [17], [18].

Physically, Figure 9 shows that a longer L lowers the equivalent bending stiffness ($\propto EI/L^3$ for doubly-clamped beams) and reduces the elastic restoring force at a given mid-span deflection, while a larger initial gap D and a larger tube radius R both increase the restoring contribution and reduce the electrostatic loading at fixed bias, raising the pull-in threshold.

For the baseline geometry, the modal-tuning range up to 60 V remains below the nonlinear pull-in threshold of about 72 V, which provides a practical bias selection margin for CNT-NEMS sensor design.

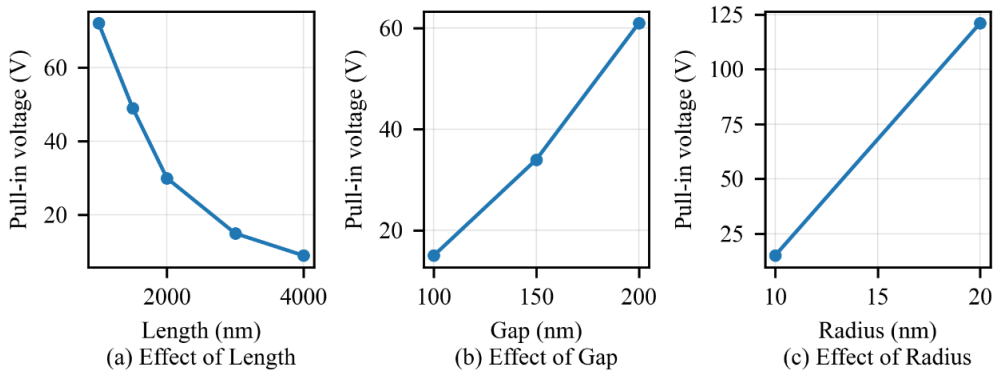

***Figure 9**. Pull-in voltage trends with respect to CNT length, initial gap, and CNT radius.*

3.8. Linear versus Nonlinear Static Response

The baseline case depicted in Figure 10 reveals a major discrepancy between modeling approaches: incorporating geometric nonlinearity raises the predicted pull-in instability threshold to approximately 72 V, compared to just 56 V when using a standard linear analysis [17].

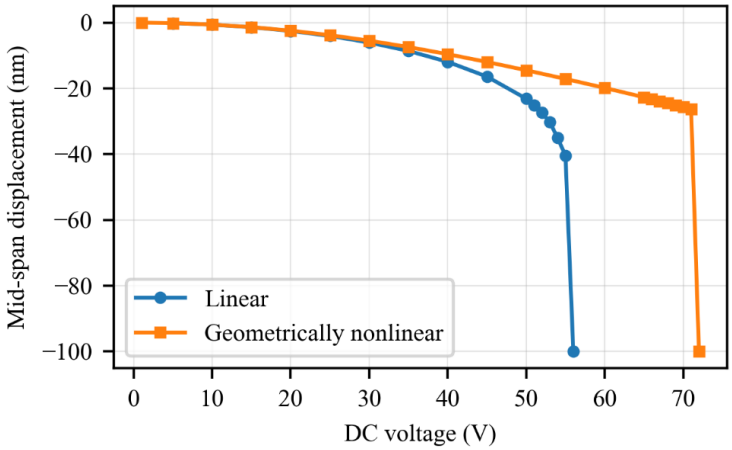

***Figure 10.** Comparison between linear and geometrically nonlinear static responses for the baseline device.*

4. Conclusions

This study established a coupled electro-mechanical finite element framework for CNT-based NEMS resonators and extended it with model validation, multimode voltage-tuning results, and pull in limited stability analysis.

The results show that the first three resonant modes stiffen markedly under DC bias, whereas the pull in threshold decreases with increasing CNT length and rises with larger initial gap and CNT radius.

These findings indicate that reliable CNT-NEMS design requires simultaneous consideration of modal tunability and nonlinear stability. The proposed framework therefore offers a practical basis for selecting geometry and bias conditions and for interpreting mass-induced frequency shifts in tunable CNT sensors.

The present continuum-shell formulation has several limitations that provide clear avenues for future research. First, the model neglects nonlocal-scale effects, material damping, and binding compliance, treating the adsorbed mass merely as a rigidly attached, lumped point mass. Second, while the single-equivalent-shell (SES) approximation successfully captures synchronous, in-phase multi-walled carbon nanotube (MWCNT) vibrations at fundamental flexural frequencies [8]–[11], it cannot resolve out-of-phase modes or individual per-wall dynamics. To address these constraints, future work will focus on: (i) incorporating nonlocal elasticity or modified-couple-stress theories to capture the small-scale regime; and (ii) developing a fully resolved multi-wall thick-shell constitutive model. This advanced model will utilize the $t_{\text{eff}} = N \times 0.34$ nm convention [10], [11] and include explicit per-wall dynamics with inter-

wall van der Waals (vdW) coupling. These enhancements will enable the analysis of high-frequency out-of-phase modes and facilitate quantitative validation against experimental MWCNT-NEMS resonator data.

Author Contributions

Dai D. Mai: Conceptualization, Methodology, Supervision, Funding acquisition, Writing - review & editing. Tuan D. Vu: Software, Formal analysis, Investigation, Writing - original draft. Si T. Do: Validation, Visualization, Data curation, Writing - review & editing.

Acknowledgments

This work belongs to the project grant No: T2025-43 funded by Ho Chi Minh City University of Technology and Engineering, Vietnam.

Conflict of Interest

The authors declare no conflict of interest.

REFERENCES

[1] K. Eom, H. S. Park, D. S. Yoon, and T. Kwon, "Nanomechanical resonators and their applications in biological/chemical detection: Nanomechanics principles," *Phys. Rep.*, vol. 503, pp. 115–163, 2011.
[2] T. Kwon, K. Eom, J. Park, D. S. Yoon, H. L. Lee, and T. S. Kim, "Micromechanical observation of the kinetics of biomolecular interactions," *Appl. Phys. Lett.*, vol. 93, art. 173904, 2008.
[3] T. Kwon, J. Park, J. Yang, D. S. Yoon, S. Na, C. W. Kim, et al., "Nanomechanical in-situ monitoring of proteolysis of peptide by cathepsin B," *PLoS ONE*, vol. 4, art. e6248, 2009.
[4] K. S. Hwang, K. Eom, J. H. Lee, D. W. Chun, B. H. Cha, D. S. Yoon, et al., "Dominant surface stress driven by biomolecular interactions in the dynamical response of nanomechanical microcantilevers," *Appl. Phys. Lett.*, vol. 89, art. 173905, 2006.
[5] C. H. Ke, H. D. Espinosa, and N. Pugno, "Numerical analysis of nanotube-based NEMS devices — Part II: Role of finite kinematics, stretching and charge concentrations," *J. Appl. Mech.*, vol. 72, pp. 726–731, 2005.
[6] M. Zheng, K. Eom, and C. Ke, "Calculations of the resonant response of carbon nanotubes to binding of DNA," *J. Phys. D: Appl. Phys.*, vol. 42, art. 145408, 2009.
[7] M. Choi, K. Eom, K. Gwak, M. D. Dai, A. Olshevskiy, and C. W. Kim, "Dynamical response of multi-walled carbon nanotube resonators based on continuum mechanics modelling for mass sensing applications," *J. Mech. Sci. Technol.*, vol. 31, pp. 2385–2391, 2017.
[8] J. Yoon, C. Q. Ru, and A. Mioduchowski, "Vibration of an embedded multiwall carbon nanotube," *Compos. Sci. Technol.*, vol. 63, pp. 1533–1542, 2003.
[9] C. Q. Ru, "Effective bending stiffness of carbon nanotubes," *Phys. Rev. B*, vol. 62, pp. 9973–9976, 2000.
[10] X. Q. He, S. Kitipornchai, and K. M. Liew, "Buckling analysis of multi-walled carbon nanotubes: a continuum model accounting for van der Waals interaction," *J. Mech. Phys. Solids*, vol. 53, pp. 303–326, 2005.
[11] C. M. Wang, V. B. C. Tan, and Y. Y. Zhang, "Timoshenko beam model for vibration analysis of multi-walled carbon nanotubes," *J. Sound Vib.*, vol. 294, pp. 1060–1072, 2006.
[12] B. Lassagne, D. Garcia-Sanchez, A. Aguasca, and A. Bachtold, "Ultrasensitive mass sensing with a nanotube electromechanical resonator," *Nano Lett.*, vol. 8, pp. 3735–3738, 2008.
[13] K. Jensen, K. Kim, and A. Zettl, "An atomic-resolution nanomechanical mass sensor," Nat. Nanotechnol., vol. 3, pp. 533–537, 2008.
[14] J. Chaste, A. Eichler, J. Moser, G. Ceballos, R. Rurali, and A. Bachtold, "A nanomechanical mass sensor with yoctogram resolution," *Nat. Nanotechnol.*, vol. 7, pp. 301–304, 2012.
[15] ANSYS Inc., ANSYS Mechanical APDL Theory Reference (Release 2023 R1) — SHELL181, TRANS126, MASS21 element formulations, Canonsburg, PA, USA, 2023.
[16] A. C. Eringen, "On differential equations of nonlocal elasticity and solutions of screw dislocation and surface waves," *J. Appl. Phys.*, vol. 54, pp. 4703–4710, 1983.
[17] M. Dequesnes, S. V. Rotkin, and N. R. Aluru, "Calculation of pull-in voltages for carbon-nanotube-based nanoelectromechanical switches," *Nanotechnology*, vol. 13, pp. 120–131, 2002.
[18] P. Chen, B. Peng, L. Ding, W. H. Xu, and Y. Q. Wang, "Simulation of singly and doubly clamped nanotube-based NEMS devices," in *Proc. ASME 2009 Int. Design Engineering Technical Conf.*, San Diego, CA, USA, 2009.

Dai D. Mai received his Bachelor of Engineering degree in Machine Design Engineering from Ho Chi Minh City University of Technology and Engineering, Ho Chi Minh City, Vietnam, in 2000, and his Master of Engineering degree in Mechanics of Constructions from the University of Liège, Liège, Belgium, in 2004. He earned his Ph.D. degree in Aerospace Information Engineering from Konkuk University, Seoul, Korea, in 2012. From 2003 to 2008, he worked as a Lecturer at Ho Chi Minh City University of Technology and Engineering, Vietnam. He then served as a Postdoctoral Research Fellow at Konkuk University, Seoul, Korea, from September 2012 to August 2013. He is currently a Lecturer at the Faculty of Mechanical Engineering, the Fundamentals of Machine Design Department at Ho Chi Minh City University of Technology and Engineering, Ho Chi Minh City, Vietnam. His current research interests include finite element analysis, coupled-field analyses, fluid-structure-interaction, piezoelectric analysis, structural-thermal analysis, electromechanical analysis, multibody dynamics simulation, and nonlinear dynamics of MEMS/NEMS.
Email: daimd@hcmute.edu.vn. ORCID: https://orcid.org/0000-0003-2932-2321

Tuan D. Vu received the Bachelor of Engineering degree in Industrial Engineering from Ho Chi Minh City University of Technology and Engineering, Ho Chi Minh City, Vietnam, in 2008, and the Master of Engineering degree in Mechanical Engineering from the same institution in 2016. He currently works at the Admissions and External Relations Department at Vietnam, Korea Binh Duong College, Ho Chi Minh City, Vietnam. His research interests include mechanical engineering, modeling and design of nano-electro-mechanical systems (NEMS), MEMS/NEMS-based sensors and actuators, and multiphysics analysis methods.
Email: ductuanv@gmail.com. ORCID: https://orcid.org/0009-0003-2245-6631

Si T. Do received his Bachelor's and Master's degrees in Mechanical Engineering from Ho Chi Minh City University of Technology, Ho Chi Minh City, Vietnam, in 2018 and 2019, respectively. Since April 2024, he has been pursuing his Ph.D. degree at the same institution. He is currently a Lecturer in the Electrical-Mechanical Department at FPT Polytechnic, FPT University, Vietnam. His current research interests focus on computational mechanics, machine design, and deep learning in engineering applications.
Email: sidt.ncs@hcmute.edu.vn / sidt3@fe.edu.vn. ORCID: https://orcid.org/0000-0002-6548-7396